Citation for published version:
Berote, J, Darling, J & Plummer, A 2015, 'Lateral dynamics simulation of a three-wheeled tilting vehicle', *Proceedings of the Institution of Mechanical Engineers, Part D: Journal of Automobile Engineering*, vol. 229, no. 3, pp. 342-356. https://doi.org/10.1177/0954407014542625

DOI:
10.1177/0954407014542625

Publication date:
2015

Document Version
Peer reviewed version

Link to publication

Berote, J., Darling, J., & Plummer, A. (2015). Lateral dynamics simulations of a three-wheeled tilting vehicle. Proceedings of the Institution of Mechanical Engineers, Part D: Journal of Automobile Engineering, 229(3), 342–356. Copyright © 2014 IMechE. Reprinted by permission of SAGE Publications.

University of Bath

Alternative formats
If you require this document in an alternative format, please contact:
openaccess@bath.ac.uk

General rights
Copyright and moral rights for the publications made accessible in the public portal are retained by the authors and/or other copyright owners and it is a condition of accessing publications that users recognise and abide by the legal requirements associated with these rights.

Take down policy
If you believe that this document breaches copyright please contact us providing details, and we will remove access to the work immediately and investigate your claim.

Download date: 06. May. 2023

Lateral Dynamics Simulation of a Three-Wheeled Tilting Vehicle

Authors: Dr J. Berote, Dr J. Darling and Prof. A. Plummer

Department of Mechanical Engineering
University of Bath
Bath, BA2 7AY
U.K.

Abstract

A novel tilting three-wheeled vehicle was developed at the University of Bath as part of an EU funded project. The space and weight savings provided by this type of vehicle could be a solution to the pollution and congestion problems seen in urban environments. The direct tilt control method originally implemented on the prototype was shown to perform well in steady state, but rapid transients were shown to potentially lead to roll-over instability. To investigate this phenomenon and design an improved controller, a multi-body model was combined with a lateral dynamics single-track model to predict both the steady state and transient behaviour. With this model it was possible to obtain an accurate representation of the kinematic and dynamic roll motion of the vehicle and the resultant weight transfer across the rear axle together with the lateral dynamics of the vehicle. The simple lateral dynamics model provided an easily understood physical representation of the system which can often be hidden in complex multi-body model. This paper presents the development of the model and its validation against data from static and dynamic tests.

Key Words: multi-body simulation, narrow track vehicle, three-wheeled vehicle, direct tilt control

Figure 1: CLEVER test vehicle at the University of Bath

1 Introduction

Narrow track vehicles can provide a significant reduction in weight and frontal area compared to ordinary cars. They also have a small road footprint as well as improved fuel efficiency. As EU car manufacturers are committed to reduce their overall fleet emissions to 130g/km by 2015 with a long term target of 95g/km for the year 2020 [1], a small vehicle with emissions equivalent to that of a motorcycle would greatly help the companies to reach these targets. In order for such a vehicle to be as comfortable and safe as a larger car, it must be relatively tall and fully enclosed. Due to the tall and narrow nature of the vehicle, it will be prone to rolling over during cornering. To prevent this from happening, it is necessary to tilt the vehicle into the turn in order to compensate for the moment caused by the lateral force generated by the tyres.

The work in this paper is related to the CLEVER vehicle, a three-wheel prototype vehicle developed at the University of Bath as part of an EU funded project between 2003 and 2006 (Figure 1).

During a steering manoeuvre the cabin of the vehicle is tilted to the desired angle using two hydraulic actuators. Although the vehicle performs well in steady state [2], transient manoeuvres can lead to the roll-over of the vehicle [3], as shown in figure 2. High lateral accelerations are not necessarily required to lead to this phenomenon.

The aim of this paper is to present a new modelling approach for an actively controlled

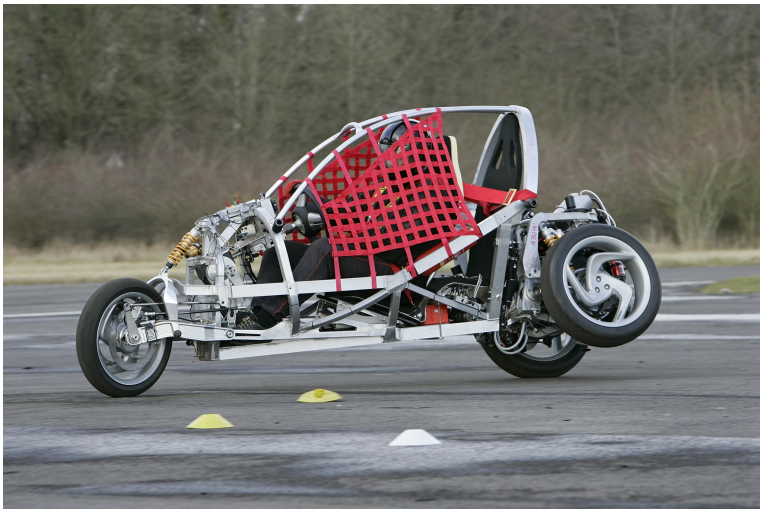

Figure 2: Lifting of inner wheel due to an aggressive steering manoeuvre

tilting three-wheeled vehicle with a tilting cabin and a non-tilting rear module. The model can be used to create a deeper understanding of the roll dynamics which are specific to this type of vehicle and dominate the overall dynamics. Furthermore it can be used as a platform to test new control approaches. The modelling approach uses a multi-body model to represent the kinematic motion and roll dynamics of the vehicle and to calculate the load on the individual wheels. These are used as inputs for an extended single-track (bicycle) model used to calculate the lateral dynamics of the vehicle. The lower frequency lateral dynamics of the model are then validated with quasi steady-state manoeuvres and the higher frequency dynamics are validated using a hardware in the loop approach with virtual steer and speed signals. This paper focuses on the vehicle model and validation. The detailed investigation of the roll dynamics leading to instability and the suggested control system are presented in [4].

A large part of the work carried out on actively controlled narrow tilting vehicles has been centered around the modelling of the vehicles in order to investigate the strategies employed to control them. An early study of tilting bicycle dynamics was presented by Sharp in [5] which he developed furter for a Motorcycle using a multi-body approach in [6]. More recently Amati et al. [7] presented a validated three wheeled tilting vehicle model using a multi-body approach, while a more general overview of tilting three wheelers can be found in [8] and [9].

Some of the earlier research on actively controlled tilting three-wheeled vehicles was performed at the University of Minnesota. Gohl et al. [10] [11] [12], Rajamani et al. [13], Piyabongkarn et al. [14] and Kidane at al. [15] [16] have published numerous papers on the subject of the control of these vehicles. A full size 2F3T (two front wheels, three tilting wheels) prototype was built in 2008 [17], where the control strategies were initially investigated on a 3DOF Bicycle model [13]. Another 2F3T protoype was developed at the Politechnic University of Turin. A study of the straight running stability carried out with a SimMechanics based multi-body model is presented in [7]. The publication also states that an active tilting system is planned for future concepts. Another narrow tilting vehicle prototype with four wheels arranged in a diamond shape was constructed at the National Chiao Tung University in Taiwan. The vehicle utilises a dual-tilt control stategy ([9], [18]) which was also investigated using a multi-body vehicle model.

1.1 The CLEVER Vehicle

The CLEVER (an acronym for Compact Low Emission VEhicle for uRban transport) consists of a tilting cabin with space for a driver and passenger and a non-tilting rear module containing the engine and ancillaries. A closed loop control system takes the vehicle velocity and steering angle as inputs to control two hydraulic actuators which tilt the cabin relative to the rear module. The control loop and hydraulic system are described in detail in sections 2.4 and 2.2. The angled joint connecting the cabin and the rear module was laid out such that a kinematic rear wheel steering angle was imposed allowing for a neutral steady state steering behaviour [2]. The front wheel is suspended with a parallel swingarm suspension system and the rear wheels have a trailing arm suspension setup. These are described in detail in section 2.3.1. The dynamics of the direct tilt controlled three-wheeler are very different from those of a conventional motorcycle in that the 'balance' function is controlled by a 'ridgidly' actuated hydraulic system acting on the rear sprung engine element. In a motorcycle the dynamics of the front wheel, the frame stiffness and tyre self centering moment are all important factors that influence the system high frequency dynamics. However

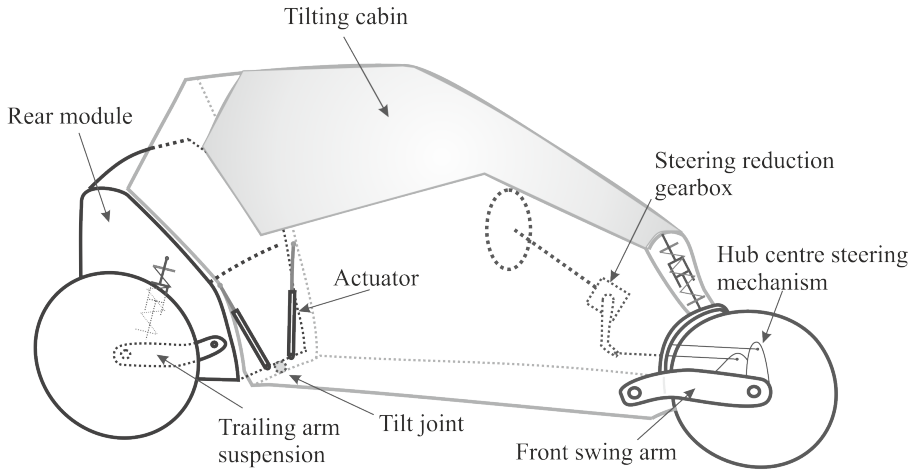

Figure 3: Schematic representation of main vehicle components

on CLEVER, the steering system that uses a reduction gearbox between the steering wheel and front wheel, the actively controlled tilt angle, and the relatively high inertia and high stiffness of the chassis mean that the concepts of 'wobble' and 'weave' do not apply, while the 'roll-over' of the rear element is a primary concern that influence the dynamics during manoeuvres. A schematic diagram of the vehicle with the principal components is shown in figure 3. The key parameters of the vehicle are listed in table 1.

2 Non-Linear Model Development

While multi-body models of tilting three-wheelers have been developed by others, the work presented here is somewhat unusual in that it combines a single track model to predict the lateral dynamics with a multi-body model to predict the lateral dynamic roll motion and the associated weight transfer across the rear axle. Although these important features of the simulation model could have been predicted with a single multi-body model it was felt that a simple lateral dynamics approach provided an easily understood physical representation of the system that can sometimes be hidden in a highly complex multi-body representation.

Table 1: Specification of the CLEVER Vehicle

General	
Type	DTC tilting three-wheeler
Construction	aluminium space frame with GRP body panels
Driver control	steering wheel and pedals (car-like)
Occupants	1+1 tandem seating
Dimensions and Weight	
Length	3m
Width	1m
Height	1.35m
Wheeltrack	0.84m
Wheelbase	2.4m
Kerb Weight	350kg
Tyres and Suspension	
Front tyre	120/R17 motorcycle
Rear tyre	160/50R18 custom
Front suspension	Swingarm with adjustable shock absorber and hub centre steering
Rear suspension	Double trailing arm with roll-stabiliser and adjustable shock absorbers
Rake / Trail	17 °/ 91mm
Steering ratio	12:1
Engine and Transmission	
Engine	230cc BMW C1 scooter (13kW @ 9000rpm)
Transmission	CVT with differential; concentric toothed final belt drive
Performance	
0-60 km/h	7s
Top speed	100km/h
Turning circle	8-9 m
Safety	
Passive	Energy absorbing safety cage with driver airbag and 3 point seatbelt
EuroNCAP	$\star\star\star$

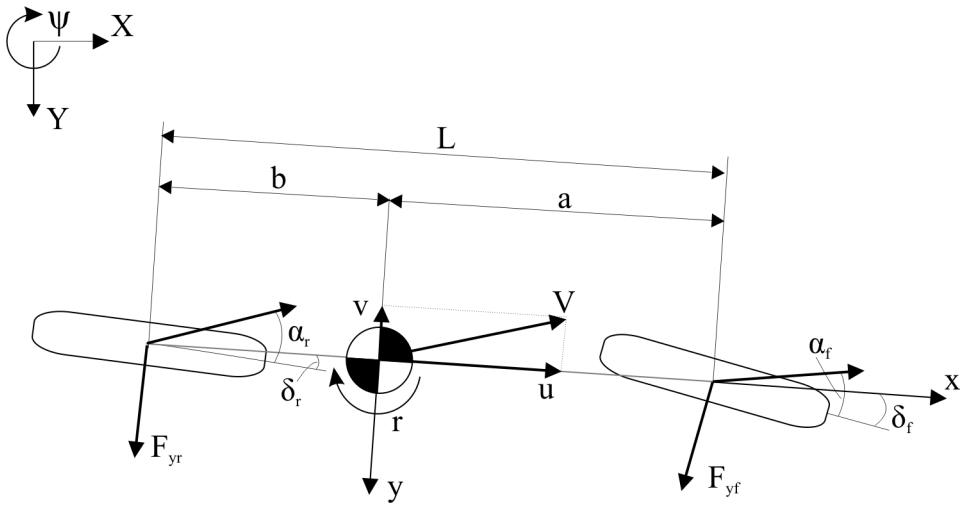

Figure 4: Bicycle model

2.1 Lateral Motion Dynamics

The slip angles at the front and rear tyres are estimated using a single-track (bicycle) model of the vehicle, where the total force produced by the rear tyres is combined in a single component. This is permissible as the rear track width is small compared to the turning radius. As this study focuses on the vehicle dynamics at constant velocity, pure slip conditions were assumed. Fore and aft weight transfer resulting from acceleration, braking and aerodynamic drag have been ignored. The tyre model is then expanded to use non-linear tyre characteristics and transient state dynamics are incorporated.

2.1.1 Equations of Motion

The 'bicycle' model is often used for linear analysis where steer δ and slip α angles are restricted to fairly small angles. This allows the variation in geometry to remain linear ($\cos\alpha \approx 1$ and $\sin\alpha \approx \alpha$ and similarly for the steer angle δ). However, a model such as the one shown in figure 4 lacks body roll and load transfer and therefore limits the theory to steady state scenarios where the roll moment remains small. This restriction is overcome by using the load transfer across the rear axle obtained through the multi-body model described in section 2.5

From the model shown in figure 4, the equations of motion are given by equations 1 and 2. The front side force F_{yf} is generated through sideslip α_f and camber γ_f, whereas the rear side force F_{yr} is generated principally through the rear tyre slip angle α_r. The resulting lateral tyre forces are a function of the vertical tyre load F_z, sideslip α and camber γ (equations 3 and 4) and are obtained through Pacejka's 'Magic Formula' as discussed in sections 2.1.2 and 2.1.3. The vertical loads and camber at the individual wheels come from the multi-body model. The slip angles are a result of the difference between the tyre direction and its velocity. The equations that describe this are equations 5 and 6. Note the rear steer term δ_r in equation 6, caused by the additional steer due to the inclination of the tilt axis [2].

$$m(\ddot{y} + \dot{x}\dot{\psi}) = F_{yf} + F_{yr} \tag{1}$$

$$I_z\ddot{\psi} = aF_{yf} - bF_{yr} \tag{2}$$

$$F_{yf} = f\left(F_{zf}, \alpha_f, \gamma_f\right) \tag{3}$$

$$F_{yr} = f\left(F_{zr}, \alpha_r, \gamma_r\right) \tag{4}$$

$$\alpha_f = \delta_f - \tan^{-1}\left(\frac{\dot{y} + a\dot{\psi}}{\dot{x}}\right) \tag{5}$$

$$\alpha_r = \delta_r - \tan^{-1}\left(\frac{\dot{y} - b\dot{\psi}}{\dot{x}}\right) \tag{6}$$

2.1.2 Rear Tyre Model

The rear tyres were modelled based on Pacejka's 'Magic Formula' or semi-empirical tyre model for car tyres. Considering lateral motion of the vehicle only, the effects of fore and aft load transfer resulting from braking, accelerating and air drag have been omitted. The Similarity Method [19] was used to estimate the parameters from the measured vertical tyre load. This method is based on the observation that the pure

slip curves remain approximately similar in shape when the tyre runs at conditions that are different from the reference condition. The reference condition is defined as the state where the tyre runs at its nominal load (F_{z0}) at camber angle equal to zero ($\gamma = 0$), free rolling and on a given road surface (μ_0). Suggested values from Pacejka's tyre model [19] were adopted, and the similarity method was used to derive the tyre characteristics at the operating load for the rear tyres on CLEVER (1350N) and compared to the characteristics at the nominal load F_{zo} given in [19] of 3000N. The parameters used are listed in table 2.

F_{zo}	3000N	C	1.3	c_1	8	μ_0	1
F_z	1350N	E	-1	c_2	1.33		

Table 2: Rear tyre magic formula parameters

The cornering stiffness is given as a function of the wheel load:

$$C_\alpha = c_1 c_2 F_{zo} \sin\left(2\tan^{-1}\left(\frac{F_z}{F_z o}\right)\right) \tag{7}$$

The peak factor for the side force is given by:

$$D_o = \mu_0 F_{zo} \tag{8}$$

The stiffness factor is given by:

$$B_o = \frac{C_\alpha}{C D_o} \tag{9}$$

Finally, the side force at nominal load F_{zo} is given by:

$$F_{yo} = D_o \sin[C\tan^{-1}(B_o x - E(B_o x - \tan^{-1} B_o x))] \tag{10}$$

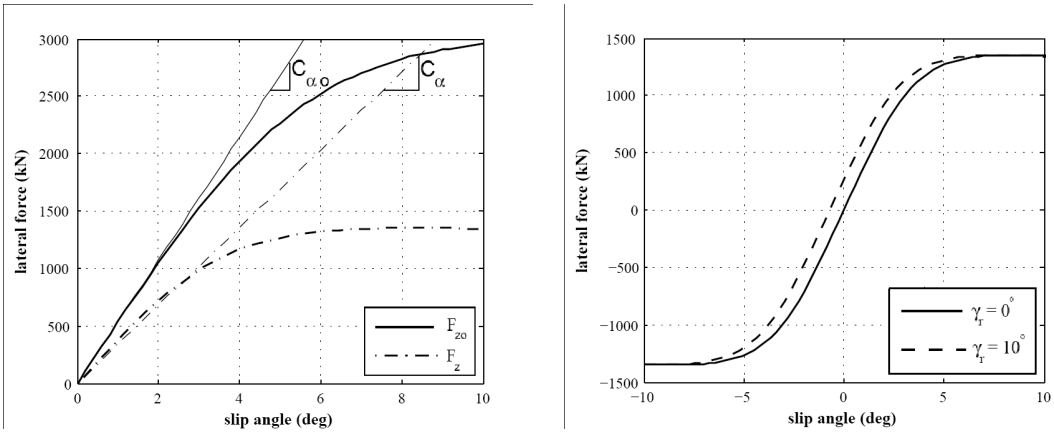

(a) (b)

Figure 5: Using the similarity method to adapt F_{yr} to a new load (a) and to introduce a camber angle (b)

where $x = \tan\alpha$.

The wheel load affects both the peak level (where the saturation of the curve takes place) and the slope where $\alpha_r \to 0$ i.e. the slip stiffness C_α. The first effect is obtained by multiplying the original characteristic equation by the ratio F_z/F_{zo}. This results in the new function:

$$F_{yr} = \frac{F_z}{F_{zo}} F_{yo}(\alpha_{eq}) \tag{11}$$

The second step in the manipulation of the original curve is the adaptation of the slope at $\alpha = 0$ which is achieved by scaling the slip angle to give an equivalent slip angle:

$$\alpha_{eq} = \frac{F_z o}{F_z} \alpha_r \tag{12}$$

The resultant transformation in the F_{yr} against α_r characteristic curve is shown in figure 5 (a).

As the rear module rolls, small levels of camber thrust will be introduced as a result of the rear wheel camber $\gamma_r = \phi$. For small angles the camber thrust generated by

the rear tyres can be approximated by the product of the camber stiffness C_γ and the camber angle [19]. This results in a horizontal shift S_h of the α_r against F_{yr} curve equivalent to:

$$S_h = \frac{C_{\gamma_r}(F_z)}{C_{\alpha_r}(F_z)}\gamma_r \tag{13}$$

This gives the equivalent slip angle α_{eq} (12) where α_r is replaced with $\alpha_r + S_h$. The resultant shift in lateral force for a given slip angle is shown in figure 5 (b).

2.1.3 Front Tyre Model

The non-linear force description of the front motorcycle tyre makes use of a simplified version of the magic formula for motorcycle tyres [19].

$$\begin{aligned}
F_{yf} &= D\sin[C\tan^{-1}(B(\alpha' + S_H))] + S_V && (14)\\
C &= d_8 && (15)\\
D &= \frac{d_4 F_z}{1 + d_7\gamma^2} && (16)\\
B &= \frac{C_\alpha}{CD} && (17)\\
S_{Hf} &= \frac{C_\gamma \gamma'}{C_\alpha} && (18)\\
S_V &= d_6 F_z \gamma' && (19)\\
S_H &= S_{Hf} - \frac{S_V}{C_\alpha} && (20)
\end{aligned}$$

The values for the parameters involved have been listed in table 3. The parameters $d_4 - d_8$ relating to the non-linear region of the slip - lateral force curve were taken from Pacejka's tyre model [19]. Figure 6 shows the effect of camber on lateral force for the front tyre.

C_α	$9.74\ F_z$	d_4	1.2	d_7	0.15
C_γ	$0.86\ F_z$	d_6	0.1	d_8	1.6

Table 3: Front Tyre Magic Formula Parameters

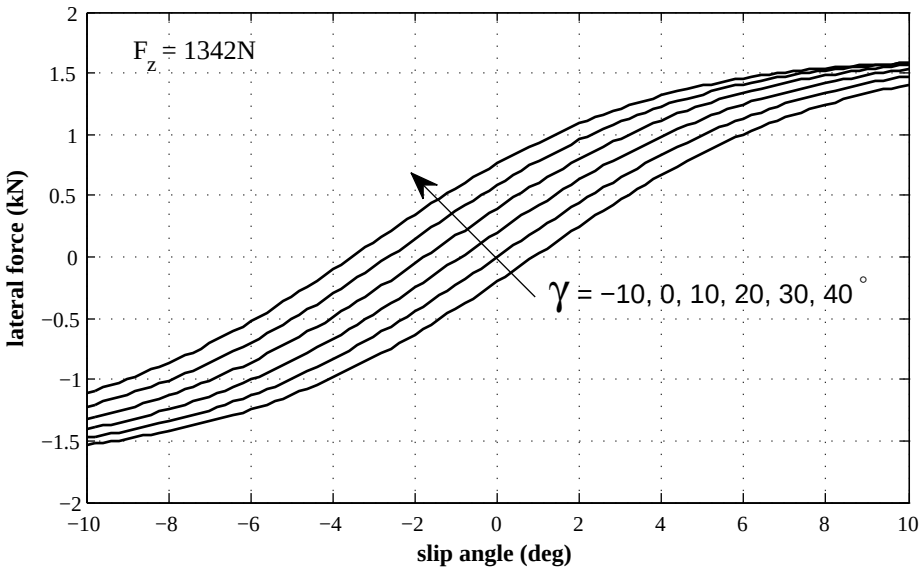

Figure 6: Effect of camber on lateral force for the front tyre

2.1.4 Single Contact Point Transient Tyre Model

As the transient lateral forces play an important role in this study, tyres with a first order lag side force response will be introduced. The relaxation length of a tyre is the distance a wheel has to travel to reach 63 % of the steady state force [20] and is denoted as σ. The relaxation length for the camber angle has been shown to be negligible [20], [19]. The following equations describe the generation of the transient slip angles $\alpha_f^{'}$ and $\alpha_r^{'}$ and resulting lateral force:

$$\alpha_f = \frac{\sigma}{\dot{x}}\dot{\alpha}_f^{'} + \alpha_f^{'} \tag{21}$$

$$\alpha_r = \frac{\sigma}{\dot{x}}\dot{\alpha}_r^{'} + \alpha_r^{'} \tag{22}$$

Figure 7 shows the normalised lateral force response or lateral acceleration response to a step steer input with and without lagged tyres. The steady state slip angles α_f and α_r are then substituted for the transient slip angles $\alpha_f^{'}$ and $\alpha_r^{'}$ as inputs for the magic formula.

2.2 Tilt Control Valve and Actuator Dynamics

A schematic diagram of the hydraulic valve and actuator system is shown in figure 8.

The actuator motion is controlled by a proportional directional control valve. The flow through the valve [21] is defined as:

$$q_1 = C_e(x_v - x_0)\sqrt{P_s - P_1} \tag{23}$$

$$q_2 = C_e(x_v - x_0)\sqrt{P_2 - P_r} \tag{24}$$

Where C_e is the valve coefficient and x_0 is the valve overlap. The actuator flow is given by:

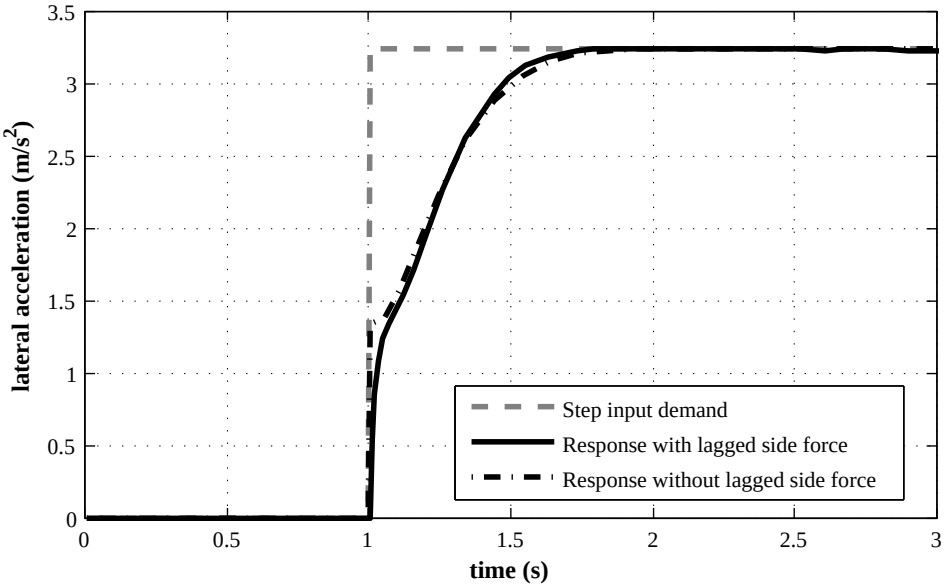

Figure 7: Example of lateral acceleration response to a step steer input using a tyre model with and without lagged side force

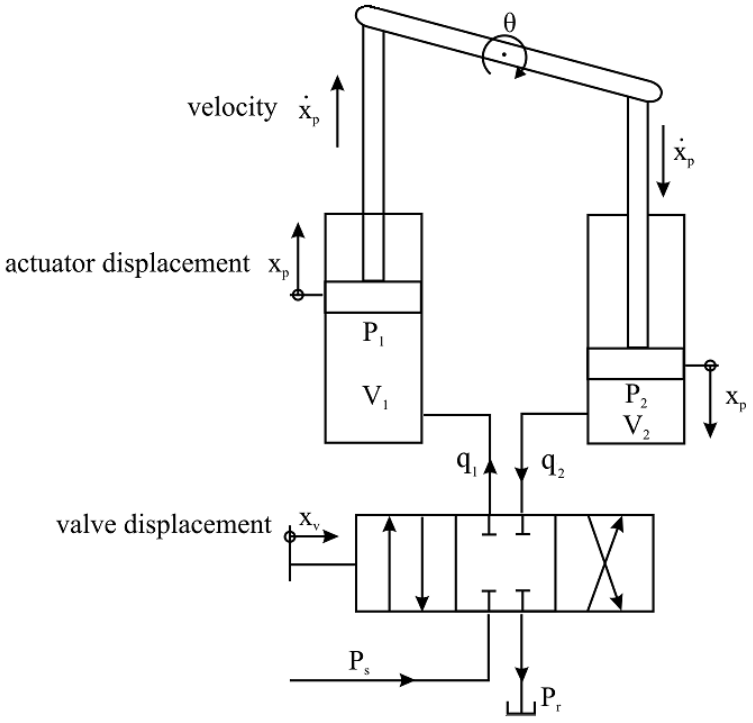

Figure 8: Representation of the valve and actuator system

$$A_p\dot{x}_p = q_1 - q_{c1} \tag{25}$$

$$A_p\dot{x}_p = q_2 + q_{c2} \tag{26}$$

where q_c is the flow into the volume due to the effect of increases in pressure. Therefore:

$$q_{c1} = \frac{V_1}{\beta_e}\frac{dp_1}{dt} = \frac{V_1}{\beta_e}sP_1 \tag{27}$$

$$q_{c2} = \frac{V_2}{\beta_e}\frac{dp_2}{dt} = \frac{V_2}{\beta_e}sP_2 \tag{28}$$

where s is the differential operator, and V_1 and V_2 are the volumes in each hydraulic cylinder which depend on the position of the actuator piston:

$$V_1 = V_0 + A_p x_p \tag{29}$$

$$V_2 = V_0 - A_p x_p \tag{30}$$

V_0 represents the volume of fluid with the actuator in the central position. Rearranging equations 25 to 28, the pressures P_1 and P_2 at either side of the piston can be shown to be:

$$P_1 = (q_1 - A_p s x_p)\frac{\beta_e}{V_1}\frac{1}{s} \tag{31}$$

$$P_2 = (A_p s x_p - q_2)\frac{\beta_e}{V_2}\frac{1}{s} \tag{32}$$

Finally, the force exerted by each actuator is given by the product of P and the piston area A_p.

2.3 Suspension Dynamics

The suspension geometry and stiffness and damping properties are vital to the dynamic behaviour of the vehicle. The rear suspension in particular has the task of reacting the forces produced by the actuators and acting as a stable platform for the tilting system. Simultaneously it should provide satisfactory ride and handling performance. The suspension parameters required for the model were taken from vehicle specifications and verified experimentally.

2.3.1 Suspension Geometry

The rear module of the vehicle uses a trailing arm suspension setup with an Öhlins spring and damper shock absorber. The geometry of the suspension was set up to give a near-linear relationship between wheel vertical movement and suspension compression by positioning the spring and damper units tangential to the arc of the trailing arm [22]. This is shown in figure 9 (b). The lever ratio in the design position is 1.38. The front suspension set-up is shown in figure 9 (a). The front wheel is attached to the chassis by two parallel swingarms and a single Öhlins spring and damper shock absorber. Figure 9 (a) also shows the hub centre steering mechanism. The lever ratio of the front spring and damper is 1.19 in the design position.

2.3.2 Parameter identification

The spring stiffnesses of the front and rear suspension units are 31kN/m and 41kN/m respectively. The damping units are adjustable in compression and rebound. The rear dampers were set to a maximum to reduce the rear module roll in transient states. To evaluate the damping coefficients with this setting, a damper was tested separately on a test bench at several operating frequencies. The data was used to obtain a linear coefficient for the damping in compression and in rebound. The results are shown in figure 10.

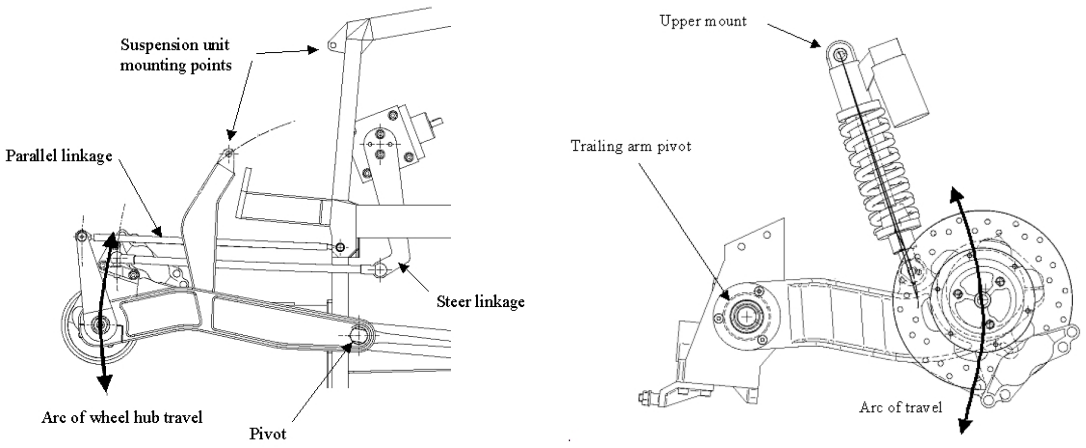

(a)Front (b)Rear

Figure 9: Front and rear suspension geometry

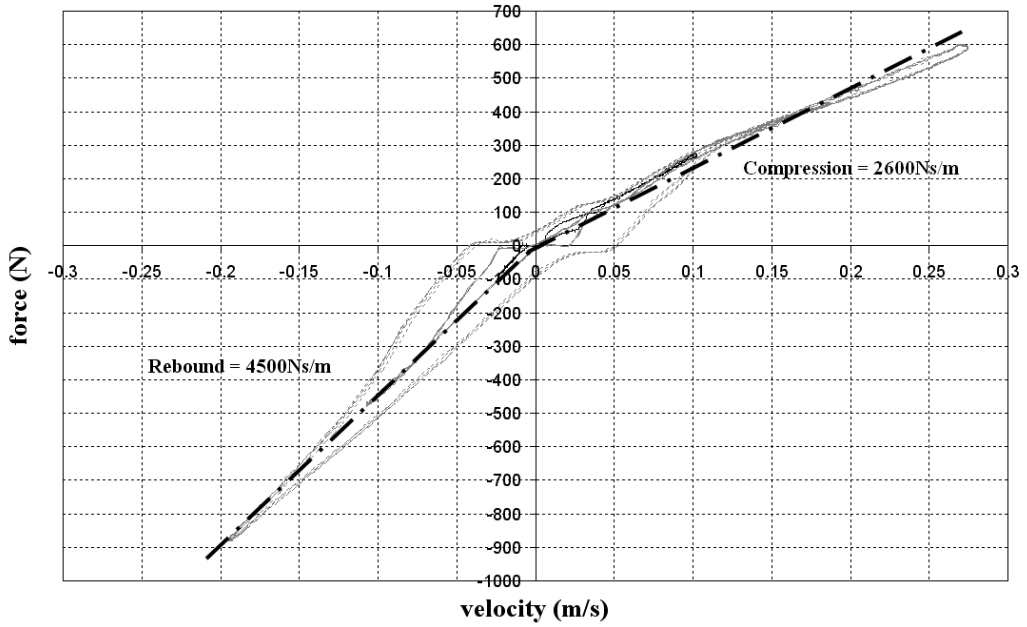

Figure 10: Results of rear damper tests and linear damping coefficient approximation

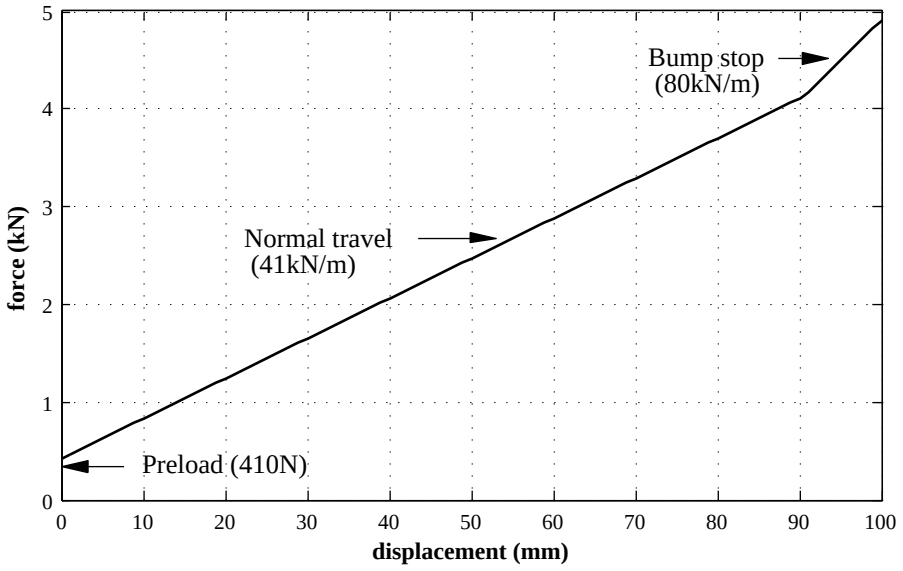

Figure 11: Effect of spring preload and bump stop stiffness for rear suspension

The damping coefficients of the rear suspension dampers in compression and rebound were approximated as 2600 Ns/m and 4500Ns/m respectively. The damping coefficient of the front shock absorber was taken as 1400Ns/m [22].

The suspension was set up with a preload of 410N. As a result, the ratio of compression and rebound travel in the design position was 60:40 mm. The effect of the pre-load and the bump stop on the suspension stiffness is shown in figure 11.

2.4 Control System

The control strategy utilises measurements of speed and steer to predict the lateral acceleration and hence the tilting angle required to balance the vehicle during cornering. This angle is referred to as the equilibrium or steady state angle, θ_{ss}:

$$\theta_{ss} = tan^{-1}\left(\frac{a_y}{g}\right) \approx \frac{a_y}{g} \tag{33}$$

Assuming that the handling characteristic remains neutral, the steer angle will be close

to the Ackerman angle. The cornering radius R can therefore be estimated from the front steer angle δ_f and the wheelbase L as shown in equation 34.

$$\tan \delta_f = \frac{L}{R} \Longrightarrow R = \frac{L}{\tan \delta_f} \tag{34}$$

The lateral acceleration can be estimated from the vehicle forward velocity as shown equation 35.

$$a_y = \omega^2 R = \frac{V^2}{R} \tag{35}$$

Equation 33, 34 and 35 can be combined to estimate the necessary steady state θ_{ss} or demand θ_d tilt angle.

$$\theta_{ss} = \theta_d = tan^{-1}\left(\frac{a_y}{g}\right) = tan^{-1}\left(\frac{V^2 \tan \delta_f}{Lg}\right) \approx \frac{V^2 \delta_f}{Lg} \tag{36}$$

Equation 36 does not take into account the non-tilting rear module, the height of the tilt-axis above the ground which results in a smaller absolute tilt angle and the non-Ackermann tyre slip angles generated at higher lateral accelerations. Furthermore, the equation was linearised for use in the controller as shown by the approximation in equation 36. In practice a gain K of 1.2 was applied to compensate for the raised tilt axis and the non-tilting rear module. The control loop for the cabin tilt position is shown in figure 12, where x_v is the valve displacement and θ_e is the error between the demand tilt angle θ_d and the relative tilt angle between the rear module and cabin θ_r.

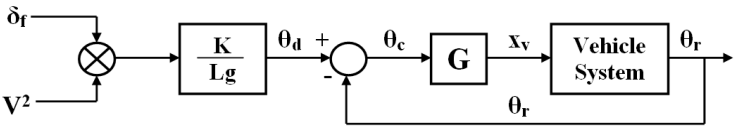

Figure 12: Tilt Position Control Loop

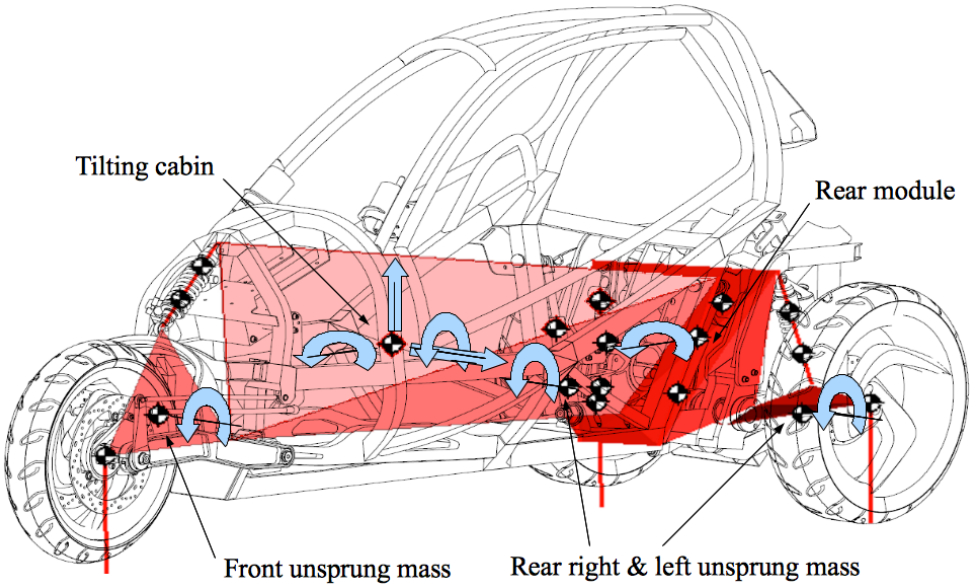

Figure 13: Vehicle multi-body model visualisation showing DOF

2.5 Integration of the Cabin and Rear Module Multi-Body Model

The software Simulink and its multi-body simulation toolbox SimMechanics were used to implement the complete model. A multi-body model was used to accurately model the relative motion of the cabin and rear-module and provide individual vertical tyre loads and camber for the lateral dynamics model described in section 2.1. Figure 13 is an image of the model as represented in the SimMechanics model visualisation mode. The image is presented as an overlay on top of an image of CLEVER such that the individual bodies can be associated with each part of the vehicle. The 8 degrees of freedom (DOF) associated with the main bodies are shown. The front and rear unsprung masses are constrained by their pivot point and move along their arc of travel (figure 9). The tilting cabin has pitch, roll, vertical and lateral degrees of freedom. The rear module has a roll degree of freedom relative to the cabin. The individual bodies and their properties are listed in table 4. The values of mass and inertia were obtained through CAD models and through measurements. The inertia of the front cabin and the rear module had to be estimated as accurate assemblies were not available. The actuators and suspension struts were also modelled as two mass systems. Their mass and inertia values have not been listed as they are small compared to the other main bodies.

The top level of the complete model is shown in figure 14 and the vehicle system parameter values are listed in table 5.

3 Vehicle Testing and Model Validation

3.1 Cabin and Rear Module Relative Roll Motion

The relative roll motion between the cabin and the rear module is dependent on the hydraulic system response. In order to test the system response, virtual speed and steer signals were generated and the resultant valve drive signal and relative tilt angle

Body	**Mass**	**Inertia** $[I_{xx} \quad I_{yy} \quad I_{zz}]$
	$[kg]$	$[kgm^2]$
Cabin	137	[14.5 200 170]
Rear Module	118	[13.3 13.3 13.3]
Driver	83	[8.2 7.3 1.4]
Front Swingarm	18	[0.43 0.60 0.77]
Rear Swingarms	15	[0.048 0.1 0.37]
Front Wheel	12	[0.27 0.54 0.27]
Rear Wheel	12	[0.27 0.54 0.27]

Table 4: Weight and inertia of main model components

Table 5: Vehicle system parameters

Lateral Dynamics		
Dist. CoG to front	a	1.56 m
Dist. CoG to rear	b	0.84 m
Front tyre slip stiffness	$C_{\alpha f}$	13.6 kNrad^{-1}
Rear tyre slip stiffness	$C_{\alpha r}$	15.7 kNrad^{-1}
Front tyre camber stiffness	$C_{\theta f}$	1.2 kNrad^{-1}
Cabin yaw inertia	I_z	235.5 kgm^2
Vehicle wheelbase	L	2.4 m
Steering ratio	i	12:1
Suspension Dynamics		
Rear suspension damping (Compression)	C_{sc}	2600 Nsm^{-1}
Rear suspension damping (Rebound)	C_{sr}	4500 Nsm^{-1}
Front suspension damping	C_f	2600 Nsm^{-1}
Rear suspension spring stiffness	K_s	41 kNm^{-1}
Front suspension spring stiffness	K_f	31 kNm^{-1}
Valve and Actuator Dynamics		
Actuator piston area	A_p	$8.043 \cdot 10^{-4}$m^2
Viscous damping of actuator	B_p	2000 Nsm^{-1}
Valve coefficient	C_e	$3.771 \cdot 10^{-7}$
Supply pressure	P_s	160 bar
Hydraulic system volume	V_t	$2.011 \cdot 10^{-4}$ m^3
Effective bulk modulus	β_e	4500 bar
Tilt gain	G	1

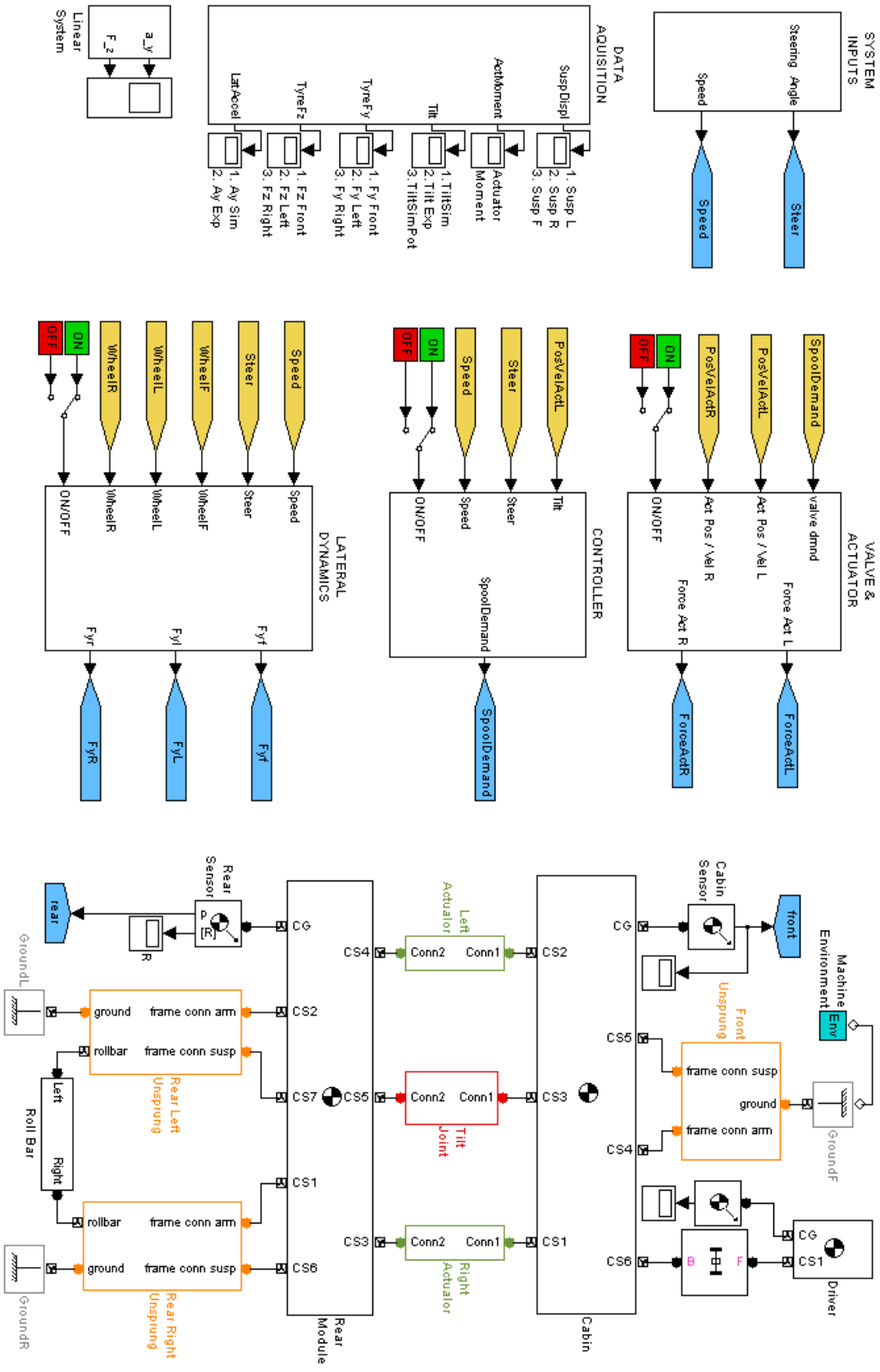

Figure 14: Top level view of multi-body model

were recorded experimentally. The system input was a sinusoidal frequency sweep from 0-8 Hz with a steering-wheel angle amplitude of ± 45°at a speed of 16.7km/h. The tilt angle was kept small in order to avoid potential damage of the vehicle at higher frequencies. Figures 15 and 16 show the recorded valve drive signal and resultant tilt angle and their simulated counterparts up to 3Hz, as this encompasses the frequency range that could practically be applied by the driver.

The valve signal represents the percentage opening, where 1 is fully open. Overall, there is a good match between the measured and the simulated results. Some deviation from the measured data can be seen at the lower frequencies, especially in the tilt angle response. It can be seen that there is a difference in the valve drive signal at these frequencies. Taking into account the 13.5% overlap of the spool, the valve opening is quite small at the lower frequencies. There would be some leakage around this point and as the flow is not yet fully developed, there is some variation in the flow coefficient C_q and the flow equation does not give such a good representation of the actual situation [21]. As a good match was obtained over the principal frequency range and inputs at very low frequencies with such a small tilt angle are unlikely to lead to dangerous transient stability states, the model was not developed further to incorporate the variation of the flow coefficient and valve leakage. Moreover, the results show a good match between the simulated and measured results at the higher frequencies that could not be tested on the moving vehicle for safety reasons.

3.2 Lateral Dynamics Tests

The CLEVER vehicle was set up with a range of sensors in order to obtain experimental data and validate the model. A number of standard dynamic tests were performed to obtain the required data. The tests were performed by a human driver, and consequently there is some variation in the forward speed. However, the theory is also said to hold approximately for quasi-steady-state situations, i.e. with moderate braking or accelerating [19]. The testing area was located on a military airfield on a tarmac surface with a marginal gradient. This meant that in steady state the vehicle still had

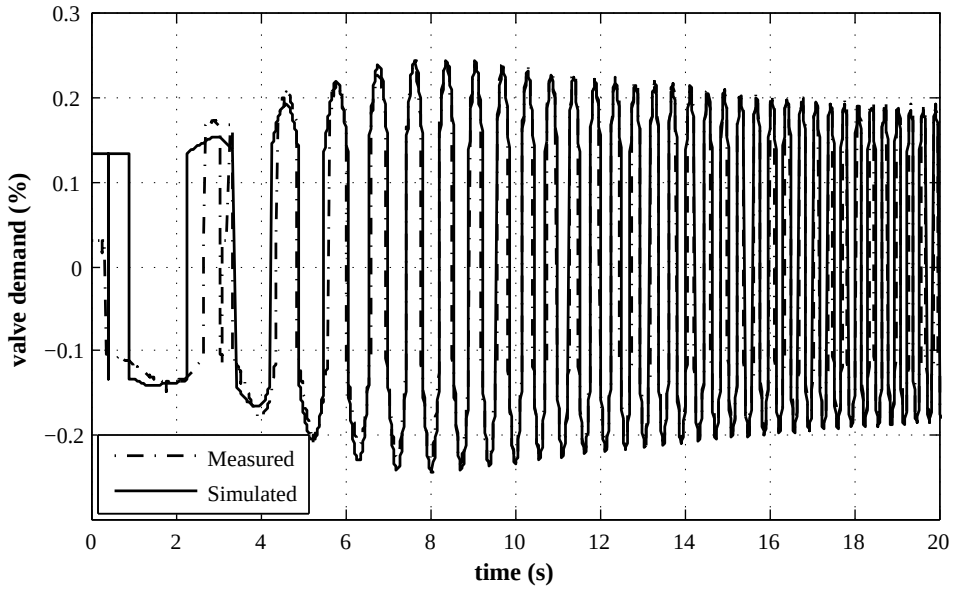

Figure 15: Resultant valve drive signal to virtual steer and speed input

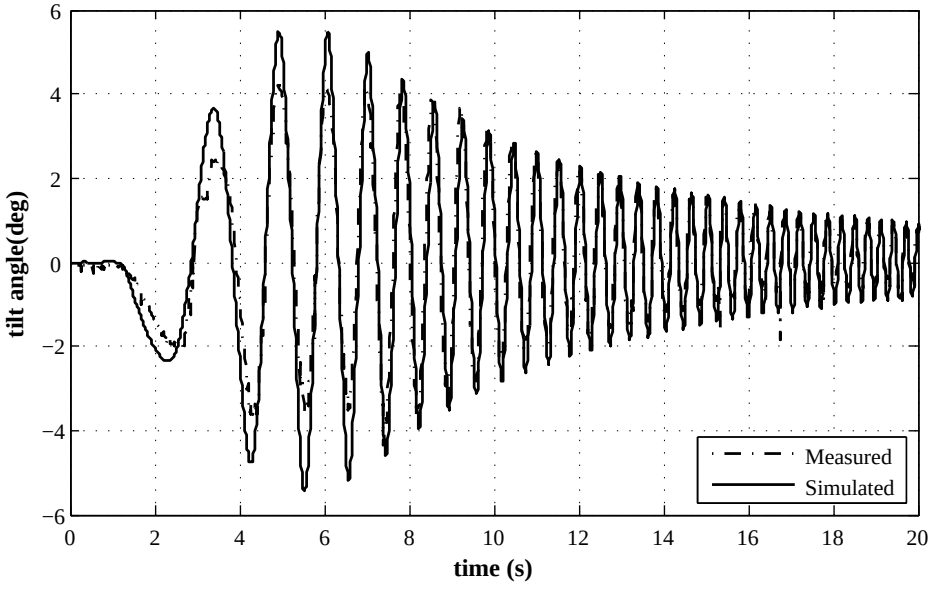

Figure 16: Tilt angle response to virtual steer and speed input

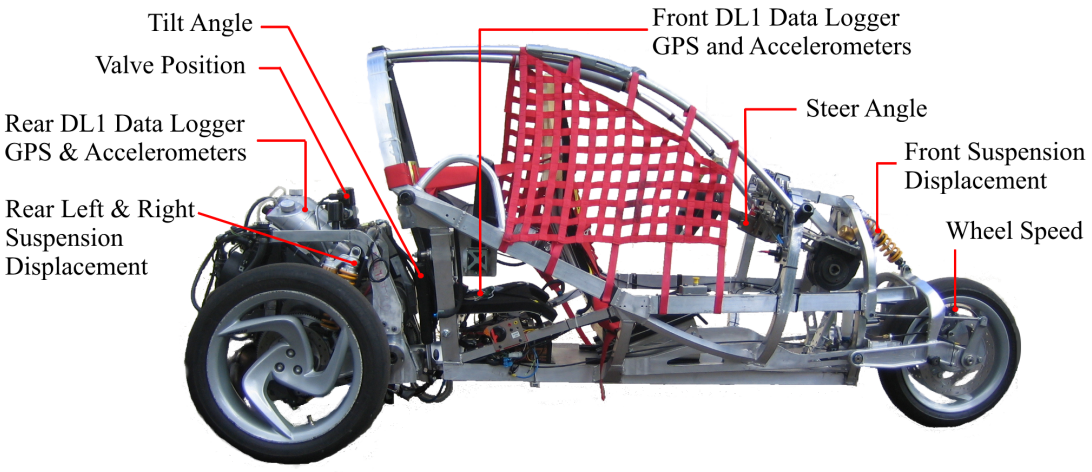

Figure 17: Sensor and data logger locations

changes in acceleration due to the slope of the test grounds. Although it was attempted to smooth out these variations in longitudinal acceleration as best as possible by the driver, they can still be seen in the test results. However, the results show a good correlation between the measured and simulated data and are mainly unaffected by these small accelerations.

3.2.1 Experimental Setup

The sensor locations are shown in figure 17. The DL1 is a data logging system with GPS receiver and dual axis accelerometers (lateral and longitudinal). The sampling frequency and accuracy of the GPS sensor and accelerometers are given in table 6. The DL1 uses the GPS data to derive several useful parameters for the analysis of the vehicle's dynamics. These are listed in table 7 along with the other measured signals. Furthermore, the DL1 utilises the accelerometer data to interpolate between the 0.1s time steps from the GPS data to obtain signals of 100Hz. The other sensors are all sampled at 100Hz, which was considered sufficient to capture all the dynamic effects that are to be investigated.

	Sampling Frequency	Range	Resolution
Accelerometers	100 Hz	2g	0.005g
GPS	10Hz	-	Position: 3m Speed : 0.1mph

Table 6: GPS and accelerometer specifications

Symbol	Description	Unit
GPS		
t	Time	[s]
v	Vehicle speed	[m·s^{-1}]
R	Cornering radius	[m]
X	X position from reference point A	[m]
Y	Y position from reference point A	[m]
$\dot{\psi}$	Yaw rate	[rad·s^{-1}]
ψ	Yaw	[rad]
Accelerometers		
a_{yc}	Acceleration measured inside the cabin	[m·s^{-2}]
a_{yr}	Acceleration measured on rear module	[m·s^{-2}]
Potentiometers		
x_f	Front suspension deflection	[m]
x_{rl}	Rear left suspension deflection	[m]
x_{rr}	Rear right suspension deflection	[m]
δ_f	Steer angle at the front wheel	[rad]
θ	Relative angle between cabin and rear module	[rad]

Table 7: Measured Test Parameters

3.2.2 Experimental Results

When the vehicle is tilting, additional tyre forces arise resulting from camber as well rear wheel steer. To get accurate results it is important to establish the absolute tilt angle at the wheel. This is the difference between the measured tilt angle and the rear roll angle. The relative tilt angle between the cabin and the rear module is measured by the linear potentiometer located between the two units.

The roll of the rear module can be measured in a number of ways. Firstly, it can be measured through the difference between the GPS measured lateral acceleration $a_{y,gps}$ and that measured by the accelerometer positioned on the rear module a_{yr}. The difference between the two signals is equivalent to the $g \sin \phi$ component measured by the accelerometer. Secondly, the roll can also be measured using the suspension displacements (and adding 7% for the tyre compliance). It was found that the accelerometer signals were significantly affected by road noise and engine noise. After filtering it was found that the suspension potentiometers gave the most accurate results. This method is therefore used to compare the measured roll to the predicted roll.

As the moment resulting from the cabin can contribute significantly to the overall moments acting on the rear module, the predicted rear module roll was compared with the measured roll with the vehicle tilting as well as with the cabin locked upright (i.e. without tilting action). Figure 18 shows the rear module roll for a figure of 8 manoeuvre with the cabin in the upright position. It can be seen that the predicted roll is significantly smoother than the measured roll. The jagged appearance of the measured roll is a result of the high friction levels in the trailing arms [4]. Furthermore, the small inclination of the testing grounds as well as irregularities in the road surface could also result in weight shifts that cause the measured roll angle to deviate from the predicted value. Nevertheless, the fit is reasonably good.

The roll angle with the vehicle driving in a figure of 8 under normal operating conditions, i.e. with tilting is shown in figure 19. Even though a number of irregularities can be seen, overall the model gives a good approximation to the roll of the rear module.

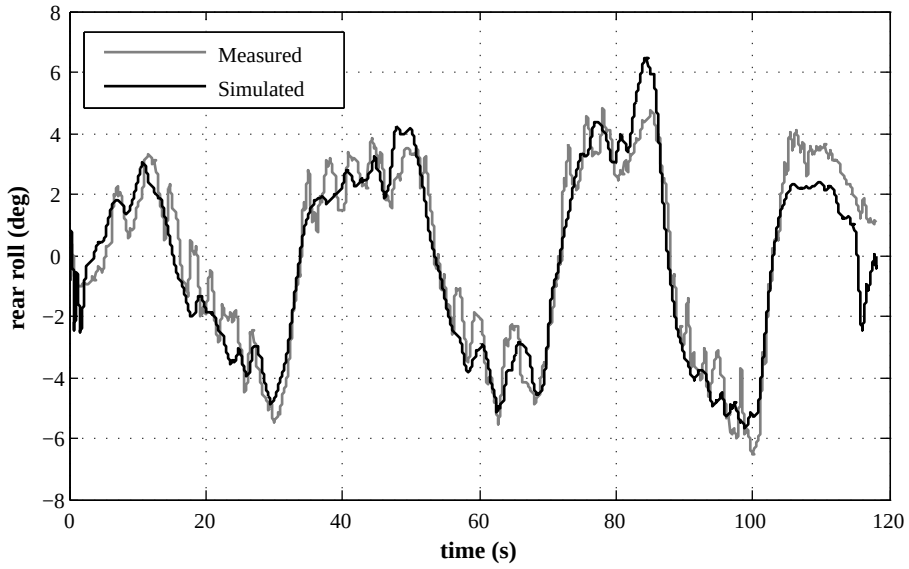

Figure 18: Rear module roll in a figure of 8 manoeuvre with the cabin locked in the upright position

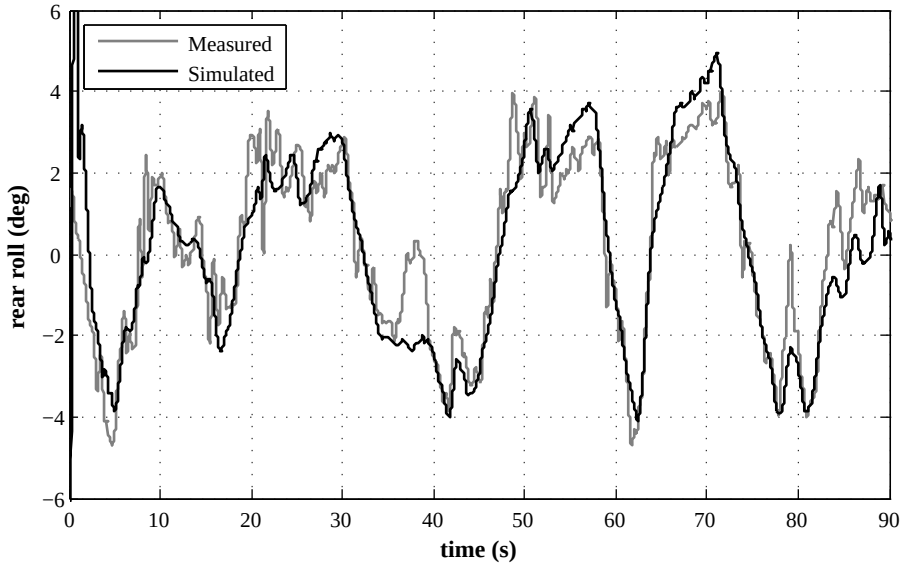

Figure 19: Rear roll whilst driving with tilting cabin

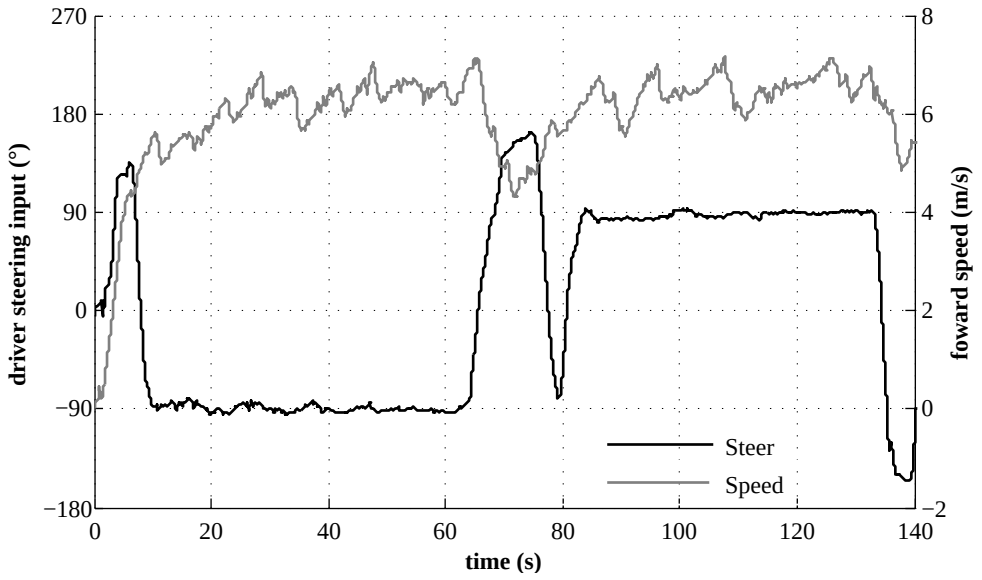

Figure 20: Steady state driving(t = 10-60 and t = 90-130 seconds) model inputs

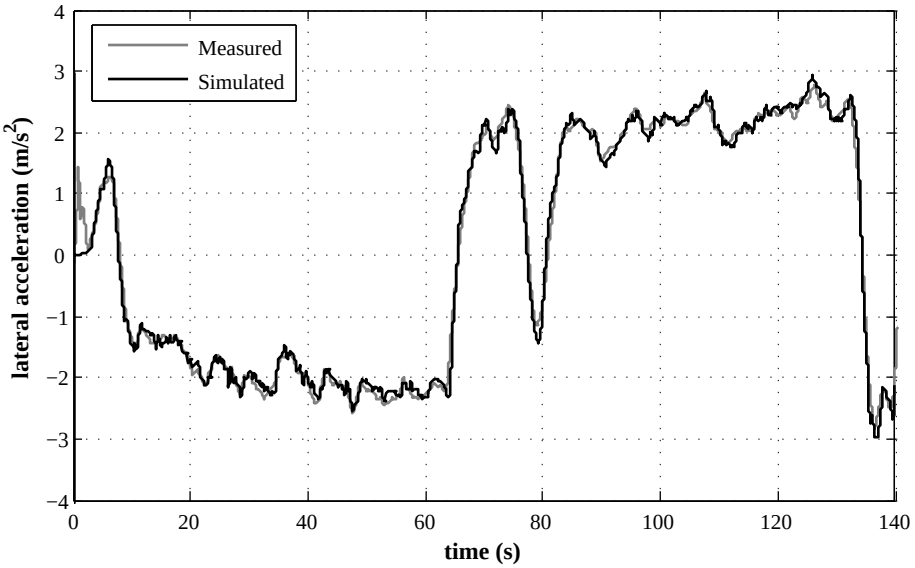

Figure 21: Measured and simulated steady state lateral acceleration (t = 10-60 and t = 90-130 seconds)

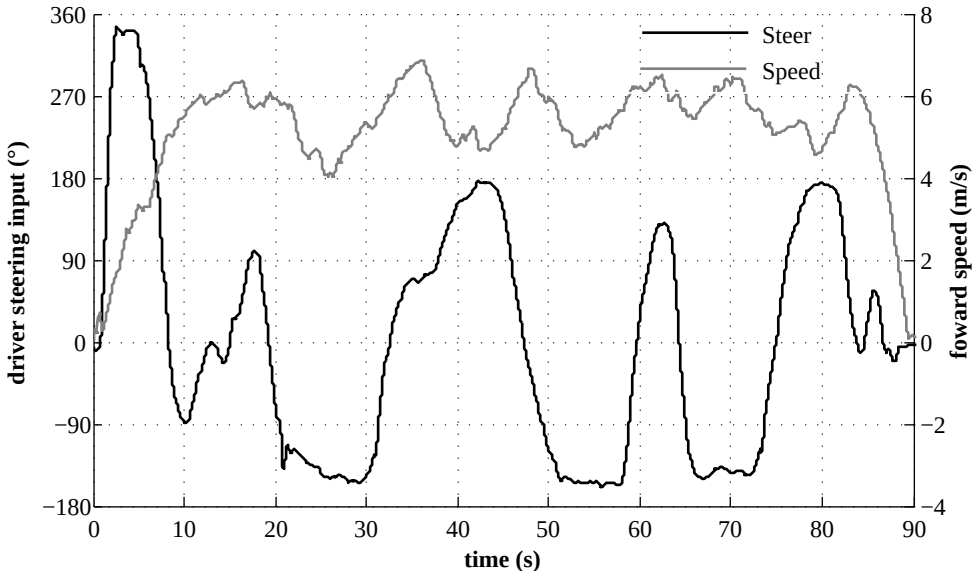

Figure 22: Model inputs for driving with moderate steering inputs

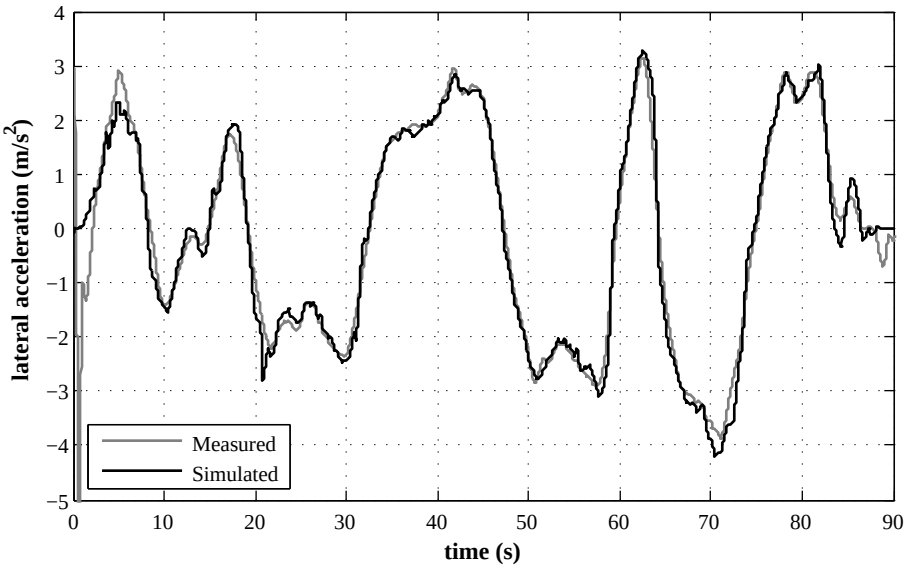

Figure 23: Measured and simulated lateral acceleration with moderate steering inputs

Figure 21 shows the resultant lateral acceleration for a steady state manoeuvre with tilting (steady state from t = 10-60 and t = 90-130 seconds) and figure 23 shows the results for the vehicle driving with moderate steering inputs. The input parameters for the model were steer and speed, shown in figures 20 and 22. It can be seen that the model gives a very accurate estimate of the vehicle lateral acceleration under the tested conditions. The measured signals were filtered with a 2 Hz lowpass filter in order to remove high frequency noise before being used as model inputs.

4 Conclusion

A multi-body model of a tilting three-wheeled vehicle using an extended single track lateral dynamics model with non-linear tyre characteristics was presented. The lateral dynamics of the complete model was validated in steady state and in quasi-steady state. Within these testing conditions, a good fit was established between the measured and the simulated dynamics with moderate steering inputs and with lateral accelerations of up to $4m/s^2$. The higher frequency roll dynamics were validated in static tests using a hardware in the loop approach and showed a good match between measured and simulated tilt angle at higher frequencies.

The simulation model presented here was used in [4] to recreate potentially dangerous driving situations, in order to obtain a better understanding of the transient dynamics leading to instability of the vehicle. Simulations showed that the load transfer across the rear module becomes critical when turning from one direction to another (i.e. the transient phase in a figure of 8 manoeuvre). This is due to the peak in initial lateral acceleration resulting from the rear steer kinematics combined with a high load transfer associated with a large tilt angle error. This can already occur at lateral accelerations below $4m/s^2$. It was shown that in order to improve the handling and stability of the vehicle, the front wheel steering has to be uncoupled from the driver steering input (active steer). The model was used as a platform to test a new type of tilt control system combining steer and tilt control inputs [4].

List of Figures

Nomenclature

A_p	actuator piston area
a	londitudinal distance of front axle to vehicle CoG
a_y	lateral acceleration
B_p	actuator damping coefficient
b	longitudinal distance of rear axle to vehicle CoG
C_e	valve coefficient
C_s	suspension damping coefficient
$C_{\alpha f}$	front tyre slip stiffness coefficient
$C_{\alpha r}$	rear tyre slip stiffness coefficient
$C_{\theta f}$	front tyre camber coefficient
F_y	lateral force on tyre
F_z	vertical force on tyre
G	tilt gain
g	gravitational acceleration
I_c	cabin roll inertia about CoG
I_r	rear module roll inertia about CoG
I_z	vehicle yaw inertia about CoG
$K_{\delta r}$	rear steer coefficient
K_f	front suspension spring stiffness
$K_{r\phi}$	roll bar stiffness
K_s	rear suspension spring stiffness
K_{xv}	spool displacement gain
L	wheel base
m	total vehicle mass
m_c	cabin mass
m_r	rear module mass
$P_{1,2}$	tilt actuator piston pressure
P_s	supply pressure
P_r	return pressure

$q_{1,2}$	flow in and out of actuator
q_c	flow into actuator due to oil compressibility
Q	actuator flow
Q_L	flow through the valve
R	corner radius
r	yaw rate
T	rear wheel track
v	lateral velocity component
V	vehicle velocity
$V_{1,2}$	fluid volume in single actuator
V_0	fluid volume with actuator in central position
V_t	total fluid volume in hydraulic system
x_p	actuator piston displacement
x_v	valve spool displacement
α_f	front tyre slip angle
α_r	rear tyre slip angle
α'	transient state slip angle
β	bulk modulus of hydraulic fluid
β_e	effective bulk modulus of hydraulic system
δ	resultant steer angle
δ_d	demand steer angle at the front wheel
δ_f	front steer angle
δ_w	driver steering angle input at the steering wheel
ΔF_z	load transfer across rear axle
ΔP_L	load pressure
ϕ	roll angle of rear module
ψ	yaw angle
σ	tyre relaxation length
θ	relative tilt angle between cabin and rear module
θ_d	demand tilt angle

θ_{ss}	steady state tilt angle of cabin
ω	rotational speed

References

[1] Anon. "Regulation (EC) No 443/2009 of the European Parliament and of the Council of 23 April 2009 setting emission performance standards for new passenger cars as part of the Community's integrated approach to reduce CO 2 emissions from light-duty vehicles (Text with EEA relevance)". Technical report, European Parliament, Council, 2009. Procedure number: COD(2007)0297.

[2] M. Barker, B. Drew, J. Darling, K. Edge, and G. W. Owen. "Steady-State Steering of a Tilting Three-Wheeled vehicle". *Vehicle System Dynamics*, 48(7):815–830, 2010.

[3] B. Drew. *Development of Active Tilt Control For A Three-Wheeled Vehicle*. PhD thesis, University of Bath, Bath, UK, 2006.

[4] J. Berote. *Dynamics and Control of a Tilting Three Wheeled Vehicle*. PhD thesis, University of Bath, Bath, UK, 2010.

[5] R.S. Sharp. "The Stability and Control of Pivoted Framed Tricycles". In *Proceedings of the 8th International Association, Vehicle System Dynamics Symposium on the Dynamics of Vehicles on Roads and Tracks (J. Karl Hedrick ed.)*, Amsterdam, 1984. Swets and Zeitlinger.

[6] R.S. Sharp, S. Evangelou, and D.J.N. Limebeer. "Advance in the Modelling of Motorcycle Dynamics". *Multibody System Dynamics*, 12:251–283, 2004.

[7] N. Amati, A. Festini, L. Pelizza, and A. Tonoli. "Dynamic Modelling and Experimental Validation of Three Wheeled Tilting Vehicles". *Vehicle System Dynamics*, 49(6):889–914, 2011.

[8] M. Barker, B. Drew, J. Darling, K. Edge, and H. Johannsen. "Review of Tilting Three Wheeled Vehicle Chassis Design". In *Proceedings of FISITA 2004 Conference*, Barcelona, Spain, 05 January 2004.

[9] J. C. Chiou and C. L. Chen. "Modeling and Verification of a Diamond-Shape Narrow-Tilting Vehicle". *IEEE/ASME Transactions on Mechatronics*, 13(6):678–691, 2008.

[10] R. Gohl, R. Rajamani, L. Alexander, and P. Starr. "The Development of Tilt-Controlled Narrow Ground Vehicles". In *Proceedings of the American Control Conference*, 2002.

[11] J. Gohl, R. Rajamani, L. Alexander, and P. Starr. "Active Roll Mode Control Implementation on a Narrow Tilting Vehicle". *Vehicle System Dynamics*, 42(5):347–372, 2004.

[12] J. Gohl, R. Rajamani, P. Starr, and L. Alexander. "Development of a Novel Tilt-Controlled Narrow Commuter Vehicle", 2006. Obtained from: http://www.cts.umn.edu/pdf/CTS-06-05.pdf on 21/09/2007.

[13] R. Rajamani, J. Gohl, L. Alexander, and P. Starr. "Dynamics of narrow tilting vehicles". *Mathematical and Computer Modelling of Dynamical Systems*, 9(2):209–231, 2003.

[14] D. Piyabongkarn, T. Keviczky, and R. Rajamani. "Active Direct Tilt Control for Stability Enhancement of a Narrow Commuter Vehicle". *International Journal of Automotive Technology*, 5(2):77–88, 2004.

[15] S. Kidane, R. Rajamani, L. Alexander, P. Starr, and M. Donath. "Experimental Investigation of a Narrow Leaning Vehicle Tilt Stability Control System". In *Proceedings of the 2007 American Control Conference*, 11–13 Jul 2007.

[16] S. Kidane, L. Alexander, R. Rajamani, P. Starr, and M. Donath. "A fundamental investigation of tilt control systems for commuter vehicles". *Vehicle System Dynamics*, 46(4):295–322, 2008.

[17] R. Moore. "U researchers advance narrow commuter vehicle concept". Obtained from: `http://www1.umn.edu/umnnews/Feature_Stories/U_researchers_advance_narrow_commuter_vehicle_concept.html` on 19/9/2007.

[18] J. C. Chiou, C. Y. Lin, C. L. Chen, and Chien C. P. "Tilting Motion Control in Narrow Tilting Vehicle Using Double-Loop PID Controller". In *Proceedings of the*

7th Asian Control Conference, pages 913–918, Hong Kong, China, 27–29 August 2009.

[19] H. B. Pacejka. *"Tyre and Vehicle Dynamics"*. Butterworth-Heinemann, 2002.

[20] V. Cossalter. *"Motorcycle Dynamics 2nd Edition"*. LuLu (Self Publishing), 2006.

[21] D. McCloy and H.R. Martin. *"Control of fluid power: analysis and design, 2nd (rev) ed."*. Ellis Horwood, 1980.

[22] M. Barker. *Chassis Design and Dynamics of a Tilting Three Wheeled Vehicle*. PhD thesis, University of Bath, Bath, UK, 2006.